JOURNAL OF MATERIALS SCIENCE **37** (2002) 2669–2684

Strength and dynamic fatigue of silicon nitride at intermediate temperatures

A. A. WERESZCZAK*, H.-T. LIN, T. P. KIRKLAND
High Temperature Materials Laboratory, Oak Ridge National Laboratory, Oak Ridge, TN 37831, USA
E-mail: awereszczak@arl.army.mil

M. J. ANDREWS, S. K. LEE‡
Caterpillar Incorporated, Peoria, IL 61656, USA

The flexure strength distributions and dynamic fatigue of GS44, NT551, and NT154 silicon nitrides were determined at intermediate temperatures ($\leq$850°C) in ambient air. GS44 and NT551 were fabricated by gas pressure sintering and had a larger volume fraction of secondary phase than the hot-isostatically pressed NT154. The inert characteristic strength for the GS44 and NT551 decreased with temperature while that for the NT154 was statistically independent of temperature. The slow crack growth exponent, N, for the GS44 and NT551 exhibited a 70–80% decrease between 700 and 850°C while the strength of NT154 was comparatively independent of stressing rate at 850°C. Associated with those changes in mechanical performances, the coefficient of thermal expansion (CTE) for the GS44 and NT551 sharply increased between 700 and 850°C while that for the NT154 did not. Although the observed change in CTE (and the temperature range where it occurred) did not have any obvious correlation with a change in inert strength at these intermediate temperatures, its presence was an indicator of a threshold temperature where dynamic fatigue resistance was compromised if the temperature exceeded it. The change in material state (and the associated temperature region for which it occurs) is linked to the equilibrium state of the secondary phase in the silicon nitride.

1. Introduction

Silicon nitride ceramics have been targeted for valve train materials in automotive and diesel industries since the early 1980's because of their excellent mechanical, thermal, corrosion-resistance properties [1–11]. These properties are expected to enable higher engine operating temperatures, lower wear rates, enhanced reliability, and longer service lifetimes. The lighter weight of these materials (about 1/3 the density of current production alloys) subsequently leads to lower reciprocating mass and improves fuel efficiency. Implementing these attributes can potentially result in better engine economy and lower emissions. For example, Rodgers *et al.* [9], quantified this difference through the examination of a 2.8 liter overhead valve V-6 engine. A 20% increase in engine speed, a 30% reduction in the maximum valve forces, and a 30% reduction in valve train friction could be realized with a change to silicon nitride valves, and this would manifest itself into as much as a 5% increase in fuel economy. Lastly, but perhaps most importantly, silicon nitride's good corrosion resistance is extremely attractive for potential engine components and its exploitation is driving many near-term application goals.

One pressing issue is the design or predictability of service performance of silicon nitride valves and other thermomechanical-bearing components in diesel engines. In order to perform such analyses, existing probabilistic life prediction codes {CARES/LIFE [12] and CERAMIC/ERICA [13]} can be readily used to combine (1) probabilistic strength and fatigue data, (2) a component's modeled thermomechanical stress state, and (3) a multiaxial failure criterion. For example, such a method and analysis have been performed by the authors with SiAlON and silicon nitride valves [14, 15].

A primary intent of this study was to generate (uncensored) strength distribution data that could be used to assess the utility of using the investigated silicon nitride ceramics in a temperature range representative of that for service for a diesel exhaust value. *The intent was not to generate (censored) Weibull strength distribution design data that could be utilized in estimating the service lifetimes of silicon nitride engines valves.* A pleasant outcome of this study was the identification or revisitation of the usefulness of dilatometry as a screening tool.

Present Address: U.S. Army Research Laboratory, Aberdeen Proving Ground, MD, USA.
‡*Present Address*: LTD Ceramics Inc., Newark, CA, USA.

0022–2461

TABLE I Description of the examined silicon nitrides

Material designation	Manufacturer	Fabrication route	Vintage
GS44	Honeywell (AlliedSignal)	Cold isostatically pressed (CIPed) and gas pressure sintered (GPS)	Late 1998–early 1999
NT551 [12, 13]	SGNIC (Norton)	Dry-pressed and GPS	Late 1997
NT154	SGNIC (Norton)	CIPed, pre-sintered, and hot isostatically pressed	≈1991

2. Experimental descriptions

2.1. Materials and specimen geometry

Three silicon nitrides were tested in this study and are listed in Table I along with their manufacturer and vintage information. Polished microstructures of each are shown in Fig. 1, and it is observed that their respective approximate average grain sizes are equivalent. Two of the silicon nitrides, GS44 and NT551, were gas pressure sintered (GPS) and the third, NT154, was hot-isostatically pressed (HIPed). The silicon nitride morphology in all three materials had a bimodal grain size and shape distribution that was comprised of long acicular grains mixed with smaller equiaxed grains. The phase content of both GS44 and NT551 consisted of 100% β-Si_3N_4 and neither grade contained a crystalline secondary phase (at least as identified by x-ray diffraction). The as-received NT154 was comprised of approximately 10% α-Si_3N_4 and 90% β-Si_3N_4 and it had polycrystalline yttrium disilicate as its secondary phase [16]. The GS44 and NT551 had greater volume fractions of secondary phase than NT154 because the latter was HIPed and inherently required less sintering aid for sintering and densification. Energy dispersive X-ray fluorescence (XRF)[§] was used to qualitatively identify that the GS44's grain boundaries contained yttrium and trace amounts (<1%) of iron, cobalt, and ytterbium and that the NT551's grain boundaries contained neodymium and yttrium and trace amounts (<1%) of calcium, cobalt, ytterbium, and lanthanum. Yttrium was known to be an additive in NT154 [16] and XRF was not used for further analysis of it.

Bend bar specimens ($3 \times 4 \times 45$–50 mm) of each material were finish ground with 320-grit diamond wheels per ASTM C1161 [17]. Transversely machined specimens were primarily studied; however, their strength distributions at a limited number of test conditions were compared with strengths measured with longitudinally machined specimens. All specimens were longitudinally chamfered. By their nature, transversely machined bars tend to produce conservative strength data that is perhaps more applicable for component design while longitudinally machined bars is reflective of the material's upper strength capability.

2.2. Test facility and procedure

Flexure testing was conducted in ambient air (20°C, relative humidity ≈40–60%) in four-point-bending using 20/40 mm, α-SiC, semi-articulating fixtures at a minimum combination of two test temperatures and two stressing rates. Initially tests were performed at 20 and 850°C; however, additional test temperatures (e.g., 500 or 700°C or both) for the GS44 and NT551 were added to the matrix for reasons that are to be described later. Flexure tests were performed at a stressing rate of 30 MPa/s to compare inert strength[¶] dependence on temperature, while a stressing rate that was several orders of magnitude slower, 0.003 MPa/s, was used to assess dynamic fatigue susceptibility. Pneumatic actuators were programmed to produce the desired loading (and corresponding stressing) rate and a resistance-heated furnace provided the desired high temperature. A linear variable differential transducer (LVDT) was used to continuously monitor push-rod displacement during testing. To assure the existence of thermal equilibrium during testing, specimens were soaked for 5–10 minutes at temperature prior to the initiation of the monotonically increasing mechanical loading (note—the LVDT reading stopped changing during this short soak indicating the achievement of thermal steady-state). Increasing load was continuously measured as a function of time, and flexure strength was calculated from the failure load and specimen and fixture geometries using ASTM C1161 [17].

The distributions of the strength data were then analyzed. An uncensored two-parameter Weibull distribution was fit to the experimental distribution of strengths for each test set using the computer program CERAMIC [6]. This program uses maximum likelihood estimation that is advocated in ASTM C1239 [18]. Reported results were uncensored because fractography was not performed to identify strength-limiting flaws in all specimens. Lastly, the fatigue exponent of each silicon nitride was determined through the examination of strength as a function of stressing rate per ASTM C1369 [19].[**]

2.3. Supplemental characterizations

Reflected light optical microscopy (RLOM), scanning electron microscopy (SEM), x-ray diffraction (XRD), and differential thermal analysis (DTA or dilatometry) were used in supplement to interpret if, and how, the material state had changed and whether or not it affected the each silicon nitride's strength distribution dependence on test condition.

Qualitative fractography and microstructural examinations were performed using RLOM[††] and SEM.[‡‡] Specimens were chosen for RLOM that had strengths equivalent in value to the characteristic strength of the test set that they were from. For example, if the characteristic strength of a data set was 500 MPa, then

[§] Lambda Research, Cincinnati, OH, USA.

[¶] The description "inert strength" represents a strength value that is unaffected by time-dependent fatigue effects. It was initially assumed in this study that the stressing rate of 30 MPa/s would be sufficiently rapid to measure each silicon nitride's inert strength.

[**] The determination of the fatigue exponent using this ASTM standard implicitly assumes that the dominant fatigue mechanism is the same at all stressing rates (i.e., time-independent).

[††] Model SZH10, Olympus, Lake Success, NY, USA.

[‡‡] S-4100 FE-SEM, Hitachi Ltd., Tokyo, Japan.

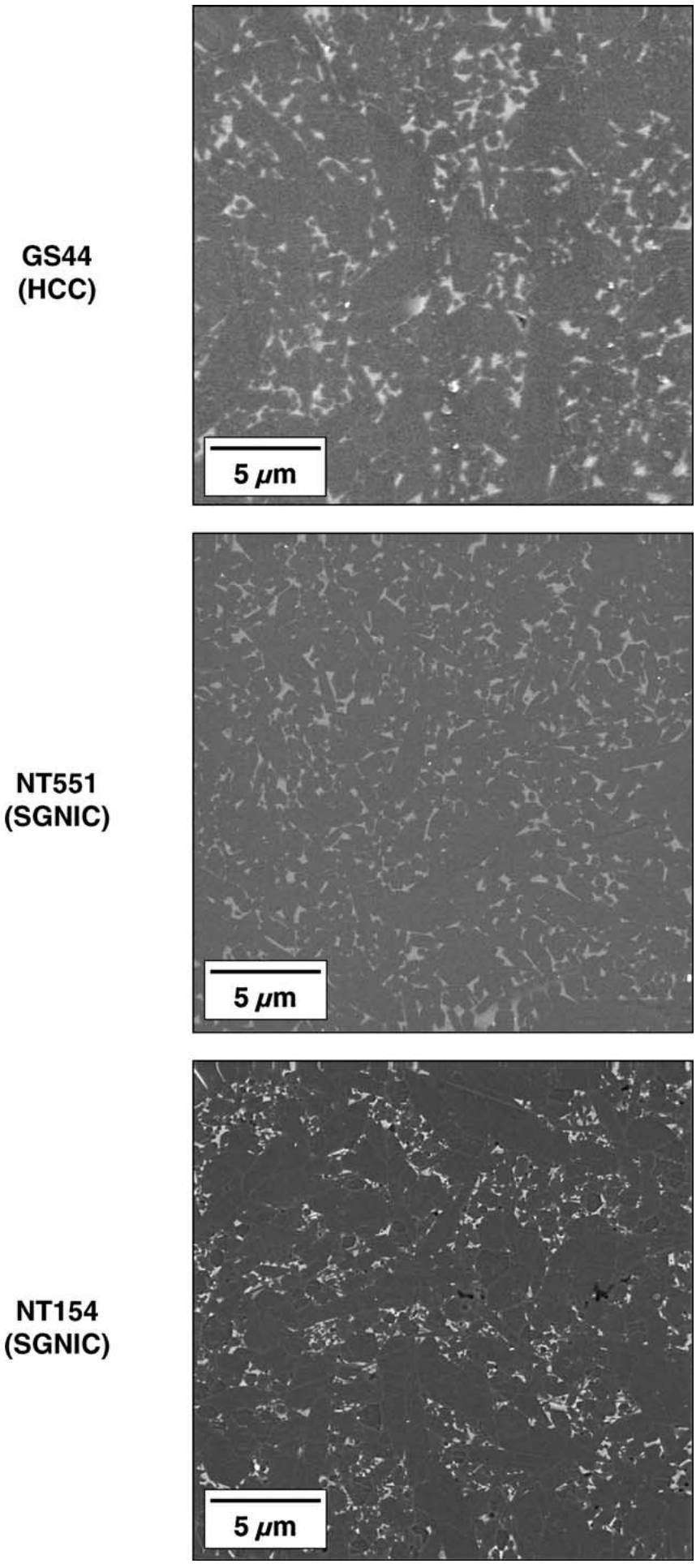

Figure 1 Comparison of the polished silicon nitride microstructures (SEM-SEI).

a specimen from that set that had a strength approximately equal to 500 MPa was examined with RLOM. Qualitative fractography was conducted with RLOM and SEM was used to investigate microstructural features of the silicon nitrides at or near the tensile surface of each examined fractured bend bar.

Qualitative phase analysis was conducted using XRD. The intent of this analysis was to identify whether or not phase changes had occurred as a consequence of the high temperature exposure/testing. The phases in as-received specimens were examined and compared to those in specimens that resulted from the longer-term testing (i.e., specimens tested at 0.003 MPa/s) at elevated temperatures (700 or 850°C or both). The specimens were scanned at a rate of 1°/min with Cu Kα radiation ($\lambda = 1.54052$ Å). The power level of the generator was 1.8 kW (45 kV and 40 mA). A continuous scan mode was employed with a step size of 0.02° over a 2θ range of 10 to 70°. Graphical analysis was only performed though in the range of 20 to 40° because the primary peaks and profile information of interest for both the Si_3N_4 and any anticipated secondary phases existed in this range.

Differential thermal analysis was conducted on all three silicon nitride specimens up to 900°C at a constant nominal heating rate of 1.7°C/minute. This analysis was added to the present study (while in progress) to further investigate observed strength distribution dependencies on temperature and stressing rate that were apparent prior to the completion of the mechanical testing. Each materials dilatation as a function of temperature was measured[§§] using a vitreous dilatometer as described in ASTM E228 [20], and referenced against a NIST standard reference material (fused silica). The continuous coefficient of thermal expansion (CTE) was determined by taking the derivative of a ninth-order polynomial fit of the elongation/temperature data and analyzed as a function of temperature. Data was collected at a rapid acquisition rate and testing was performed to a temperature (900°C) that exceeded that of primary interest (850°C); this allowed the authors to avoid misleading, high-order-polynomial-regression artifacts that can result at the extremes of the values of the independent parameter.

3. Results and discussion

3.1. Strength dependencies on temperature and stressing rate

3.1.1. Uncensored Weibull strength distributions

The fitted uncensored Weibull strength distributions for the GS44, NT551, and NT154 are shown in Fig. 2a–e), Fig. 2f–h, and 2i, respectively, along with each set's flexure strength data and ±95% confidence intervals about the maximum likelihood estimated fit. Five hundred and ninety test specimens comprised the examined matrix, and confidence estimates about the two parameters were determined, so any observed differences are reported with statistical significance. A summary of their descriptions is listed in Table II.

[§§]Holometrix Micromet, Bedford, MA, USA.

TABLE II Summary of uncensored Weibull strength distributions (ASTM C1161-B)

Material	Mach. direct.	Temp. (°C)	Stress rate (MPa/s)	No. of specimens tested	Weibull modulus	±95% Weibull modulus	Characteristic strength (MPa)	±95% Characteristic strength (MPa)
GS44[a]	Tran	20	30	12	28.9	17.5, 43.0	793	775, 811
GS44[a]	Tran	20	0.003	12	30.8	18.6, 45.9	673	658, 687
GS44[a]	Tran	500	30	15	19.1	12.6, 26.6	734	712, 756
GS44[a]	Tran	500	0.003	15	23.8	15.6, 34.0	642	626, 657
GS44[a]	Tran	700	30	15	29.8	19.5, 42.1	694	680, 709
GS44[a]	Tran	700	0.003	15	22.2	14.6, 31.2	632	616, 648
GS44[a]	Tran	850	30	11	23.7	14.0, 36.2	748	726, 770
GS44[a]	Tran	850	0.003	15	25.8	16.6, 37.0	545	532, 556
GS44[b]	Long	20	30	30	22.2	16.3, 29.0	959	941, 975
GS44[b]	Long	850	30	30	19.1	14.5, 24.2	776	759, 791
GS44[b]	Long	850	0.003	21	20.5	13.8, 29.0	590	576, 603
NT551	Tran	20	30	30	9.4	7.0, 12.3	805	772, 839
NT551	Tran	20	0.3	30	10.9	8.1, 13.9	705	679, 730
NT551	Tran	20	0.003	29	11.6	8.4, 15.3	605	584, 625
NT551	Tran	700	30	15	9.6	6.0, 14.1	593	558, 629
NT551	Tran	700	0.3	14	7.7	4.8, 11.4	530	489, 571
NT551	Tran	700	0.003	15	9.0	5.7, 13.2	532	498, 566
NT551	Tran	850	30	30	8.5	6.3, 10.9	576	550, 602
NT551	Tran	850	0.3	30	5.2	3.9, 6.7	517	479, 556
NT551	Tran	850	0.003	30	4.4	3.5, 5.5	380	352, 410
NT551	Long	20	30	32	11.9	8.6, 15.9	1038	1006, 1071
NT551	Long	850	30	27	6.3	4.6, 8.2	558	521, 595
NT154	Long	20	30	30	9.0	6.7, 11.7	706	675, 736
NT154	Long	850	30	30	9.3	6.9, 11.9	685	656, 714
NT154	Long	850	0.003	27	5.9	4.5, 7.4	618	576, 662

[a]Lot C99091. [b]Lot C98236.

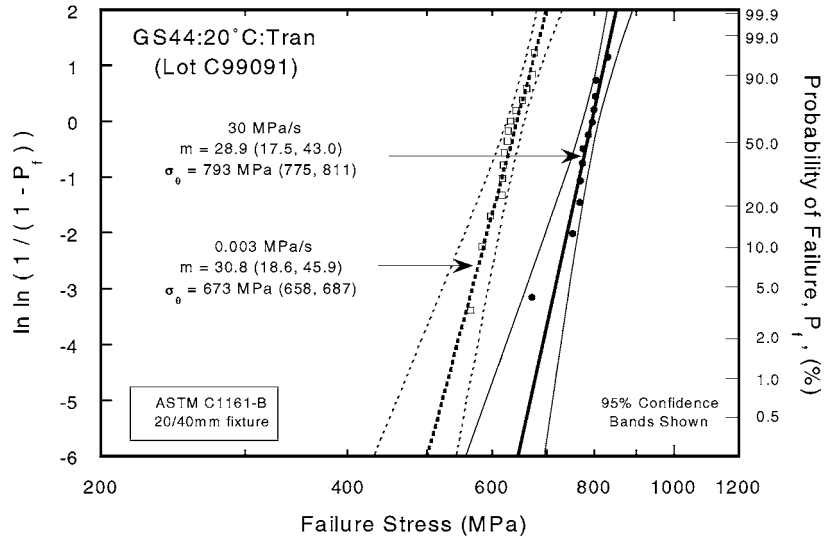

(a)

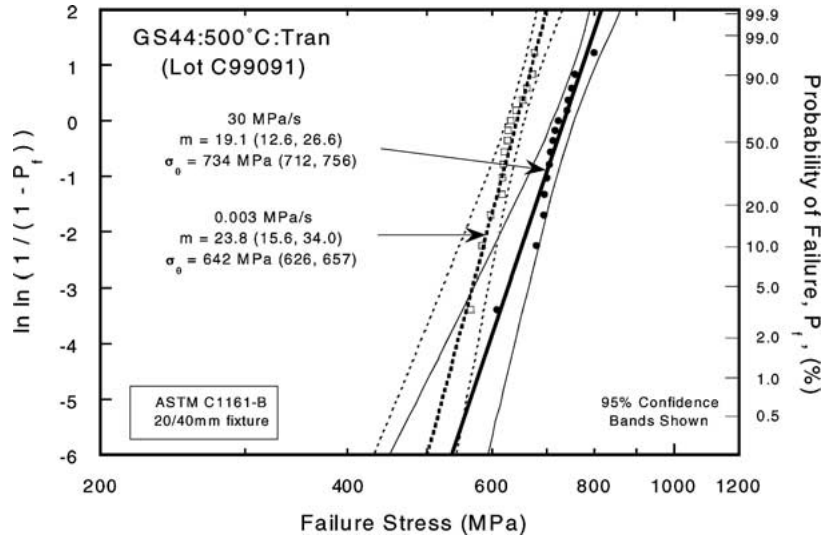

(b)

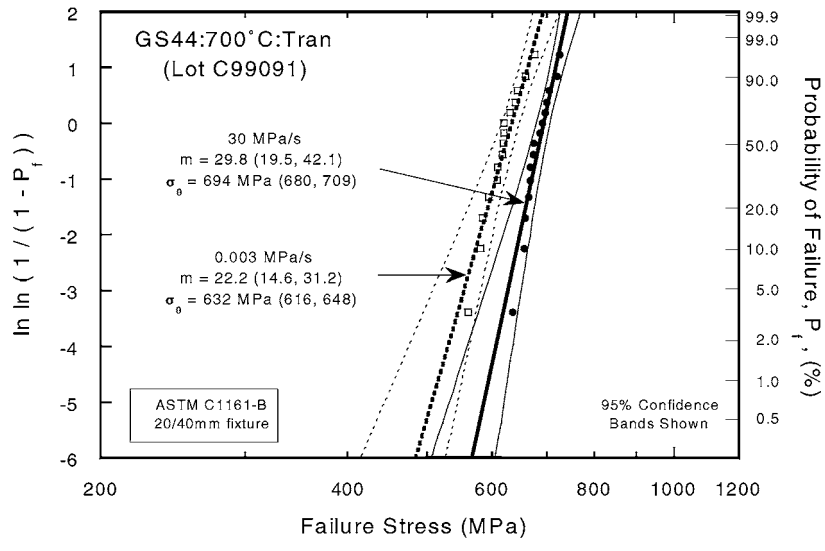

(c)

Figure 2 Probability of failure as a function of failure stress for (a–e) GS44, (f–h) NT551, and (i) NT154 at different test temperatures and stressing rates. (*Continued.*)

The characteristic strengths of GS44 tested at 30 and 0.003 MPa/s are statistically different for each of the five test conditions it was evaluated at, as shown in Fig. 2a–e. Graphically, this is portrayed by the apparent shifting of the curves between the two rates with the characteristic strength always being larger-valued when the set was tested at 30 MPa/s. Although there is a statistically significant decrease (to varying degrees) in characteristic strength for GS44 when tested at 0.003 MPa/s at all the investigated conditions, the slopes for all their

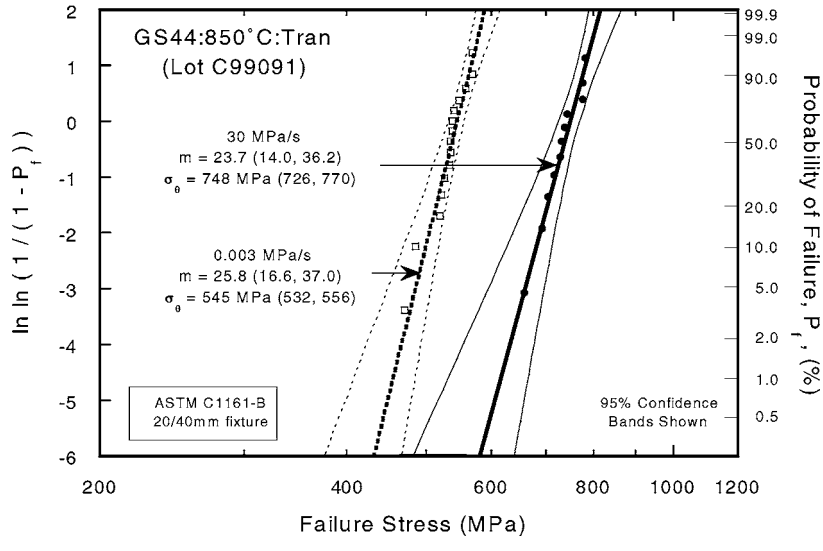

(d)

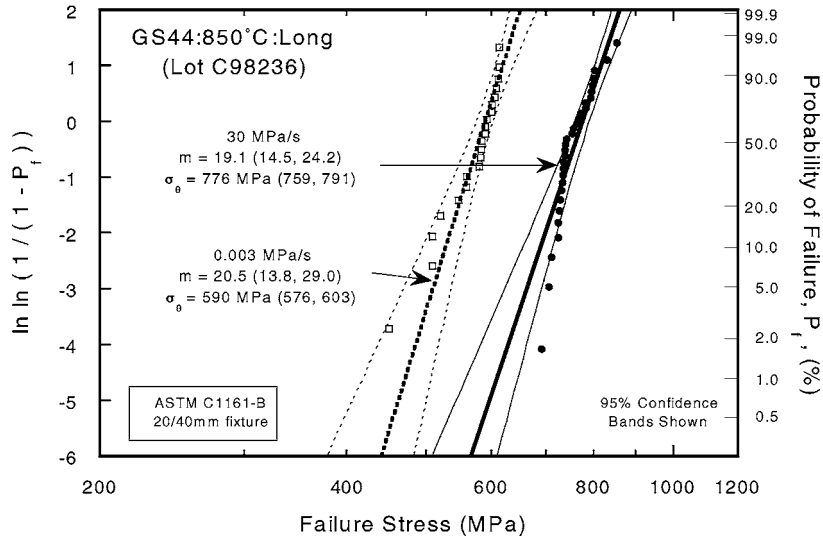

(e)

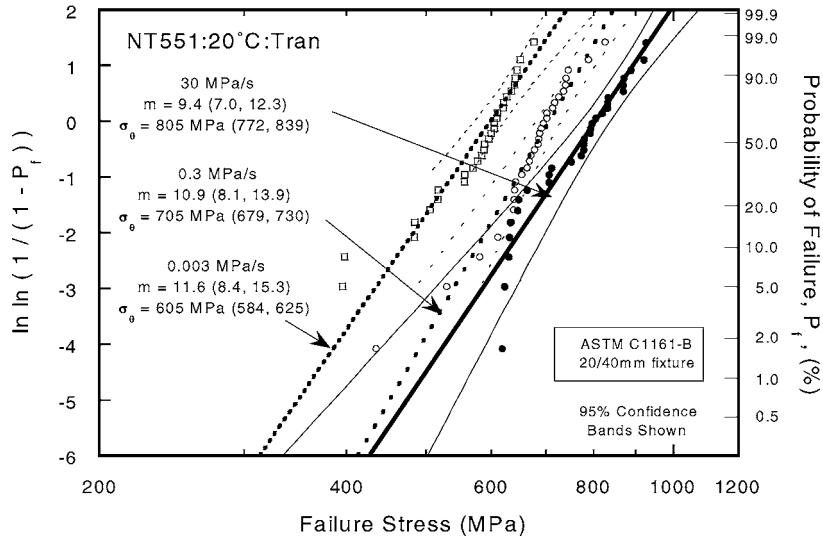

(f)

Figure 2 (*Continued.*)

conditions are statistically equivalent; namely, the uncensored Weibull modulus is apparently independent of temperature, stressing rate, and grinding orientation. Although the comparison of grinding orientation effects in Fig. 2d–e resulted from the testing of different processing lots of GS44, they still illustrate that the uncensored characteristic strength is significantly lessened when tested at 0.003 MPa/s and that perhaps the state of the material is causing this effect and that this effect is not dependent on how the specimens were machined. Furthermore, the lessening of GS44's characteristic strength at 850°C between 30 and 0.003 MPa/s

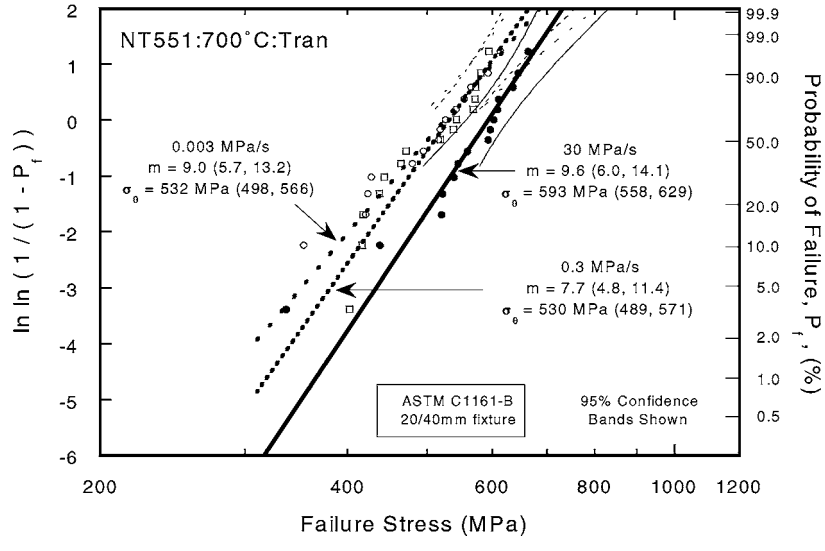

(g)

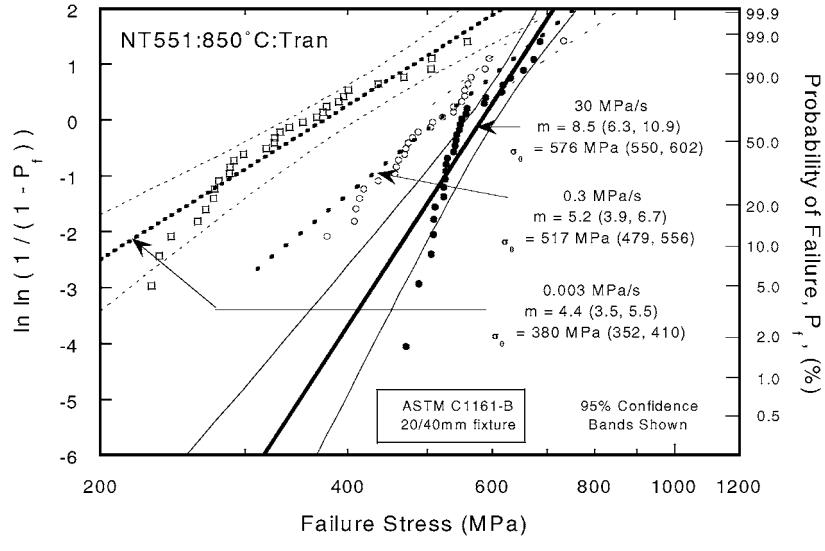

(h)

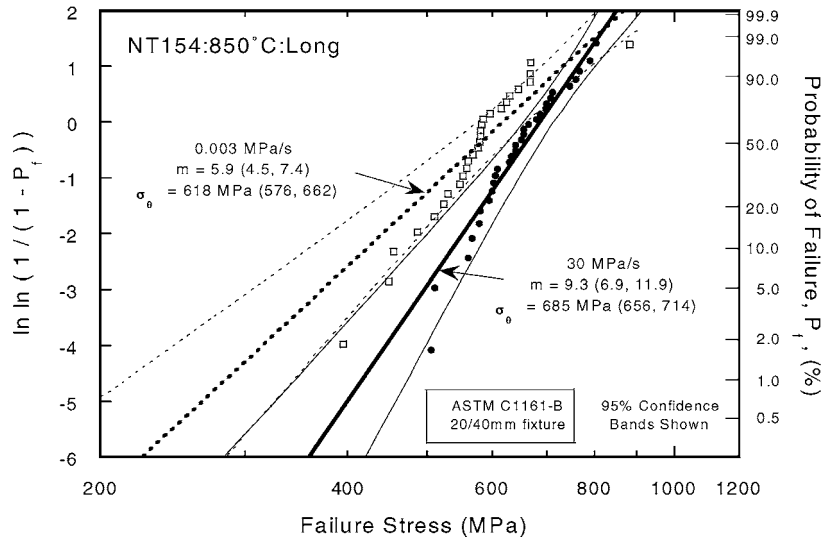

(i)

Figure 2 (*Continued.*)

is much more significant than at 700°C; this suggests that GS44 may be undergoing some change of state between 700 and 850°C, and that it is further exploited when GS44 is strength-tested at different stressing rates at 850°C.

The uncensored Weibull moduli for NT551 at 20 and 700°C, and at all investigated stressing rates, were statistically equivalent. Additionally, there was a general trend of characteristic strength decrease when NT551 was tested at slower stressing rates at both temperatures.

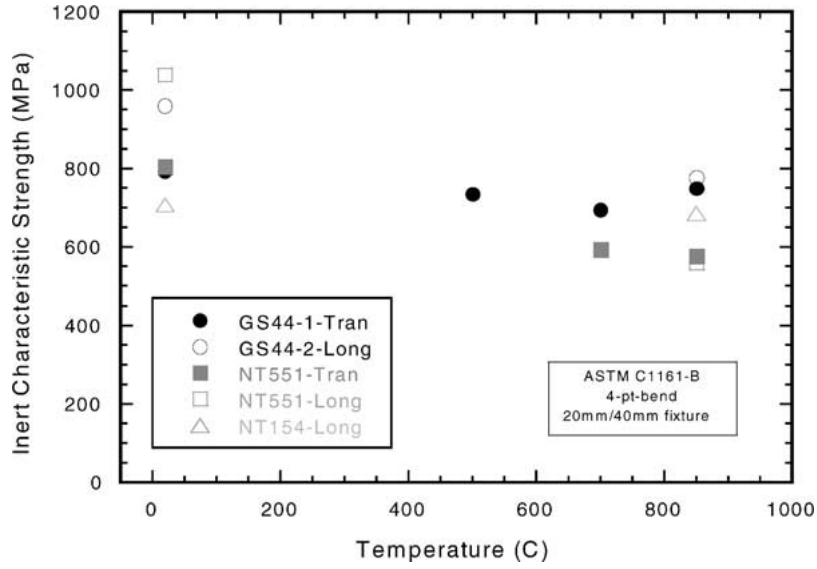

Figure 3 Inert characteristic strength as a function of temperature.

However, at 850°C, both the uncensored Weibull modulus and characteristic strength of NT551 changed when slower stressing rates were tested. These trends are graphically portrayed in Fig. 2f–h. These observations regarding the Weibull distribution changes suggest that NT551, like the GS44, may be undergoing a change in material state between 700 and 850°C, and that that change is further exploited when NT551 is strength-tested at different stressing rates at 850°C.

Unlike GS44 and NT551, there was only a statistically subtle change in the uncensored Weibull modulus and characteristic strength at 850°C when NT154 was tested at 30 and 0.003 MPa/s as shown in Fig. 2i. This suggests that if there was a change of state within NT154 at 850°C then its extent was not as dramatic as the change of state in GS44 and NT551 at the same temperature.

The uncensored inert characteristic strength as a function of temperature (see Fig. 3) showed a dependence on the grinding orientation for the GS44 and NT551. Longitudinally ground GS44 and NT551 show a large drop in their inert characteristic strength between 20 and 850°C. Transversely ground GS44 specimens showed a subtle decrease and NT551 showed a relatively large decrease in inert characteristic strength over the same temperature range. Although transversely ground NT154 bend bars were not examined, its inert characteristic strength measured with longitudinally machined bend bars showed insensitivity to temperature between 20 and 850°C. The dependencies of inert characteristic strength on temperature and grinding orientation for the GS44 and NT551; the lack of such a dependency on temperature for the NT154; and the trends described in the preceding paragraphs indicated that the strength distributions of GS44 and NT551 were somewhat similar, while those for the NT154 were different.

The increasing load as a function of LVDT displacement values were examined at all stressing rates and temperatures for all three materials, and it was consistently observed that all bend bars specimens only exhibited linear elasticity to their fracture. This indicates that none of the specimens underwent plastic deformation nor could plastic deformation have accounted for the observed strength distribution changes that were described in the preceding paragraphs. Plastic deformation of bend bars can produce an apparent lessening of flexure strength [21]; however, that influence was not present in these results.

3.1.2. Fatigue susceptibilities

The fatigue susceptibilities of GS44 and NT551 changed as a function of temperature, and their fatigue exponent values are listed in Table III along with 95% confidence intervals. The uncensored characteristic strength for the three examined silicon nitrides are shown in Fig. 4 as a function of stressing rate. Qualitatively, the slopes of the curves for the GS44 and NT551 generally decreased (i.e., an increase in the fatigue exponent—see Fig. 5) between room temperature and 700°C while the slopes had increased (i.e., a decrease in the fatigue exponent—Fig.5) at 850°C.

The apparent increase in the fatigue exponent at 700°C from that at 20°C for GS44 and NT551 is not fully understood by the authors; however, there is a process that perhaps contributes to such apparent

TABLE III Summary of uncensored dynamic fatigue exponents

Material	Machining orientation[a]	Temp. (°C)	Fatigue exponent (±95% conf.)
GS44[b]	Transverse	20	42 (35, 52)
GS44[b]	Transverse	500	70 (53, 103)
GS44[b]	Transverse	700	93 (69, 138)
GS44[b]	Transverse	850	28 (25, 33)
GS44[c]	Longitudinal	850	32 (28, 37)
NT551	Transverse	20	28 (22, 39)
NT551	Transverse	700	86 (39[d])
NT551	Transverse	850	18 (14, 24)
NT154	Longitudinal	850	75 (47, 184)

[a]320-grit per ASTM C1161. All edges longitudinally chamferred.
[b]Lot C99091.
[c]Lot C98236.
[d]Upper bound value undefined (i.e., negative value).

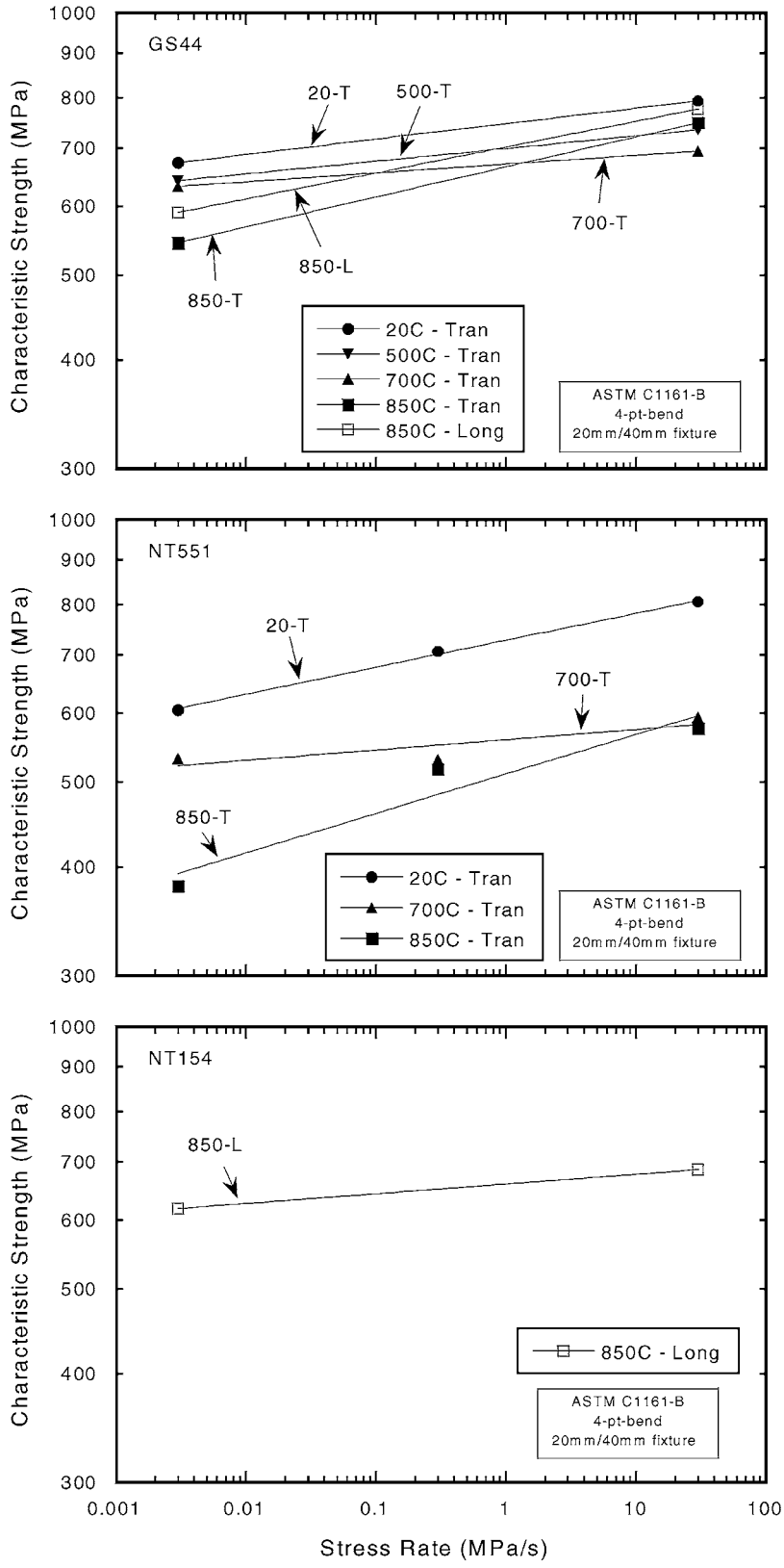

Figure 4 Characteristic strength as a function of stressing rate.

behavior. At 20°C, the relief of machining-induced residual stresses would either be non-existent or at least equally occurring when the bend bars were tested at 30 or 0.003 MPa/s. At 700°C though, the temperature may be sufficient to cause residual stress relaxation in the secondary phase and testing at 0.003 MPa/s may provide substantially more time for a (albeit viscous) secondary phase to relax greater amounts of tensile stresses. Such a process would obviously be time-dependent in this instance, and the net effect would be that the apparent fatigue resistance would be better owing to stress superposition and the situation where less tensile stress was contributing to fracture at 0.003 MPa/s than at 30 MPa/s.

The fatigue resistances of both GS44 and NT551 markedly decreased at 850°C by approximately 70–80% from that at 700°C. The dramatic change in fatigue resistance between 700 and 850C is illustrative of

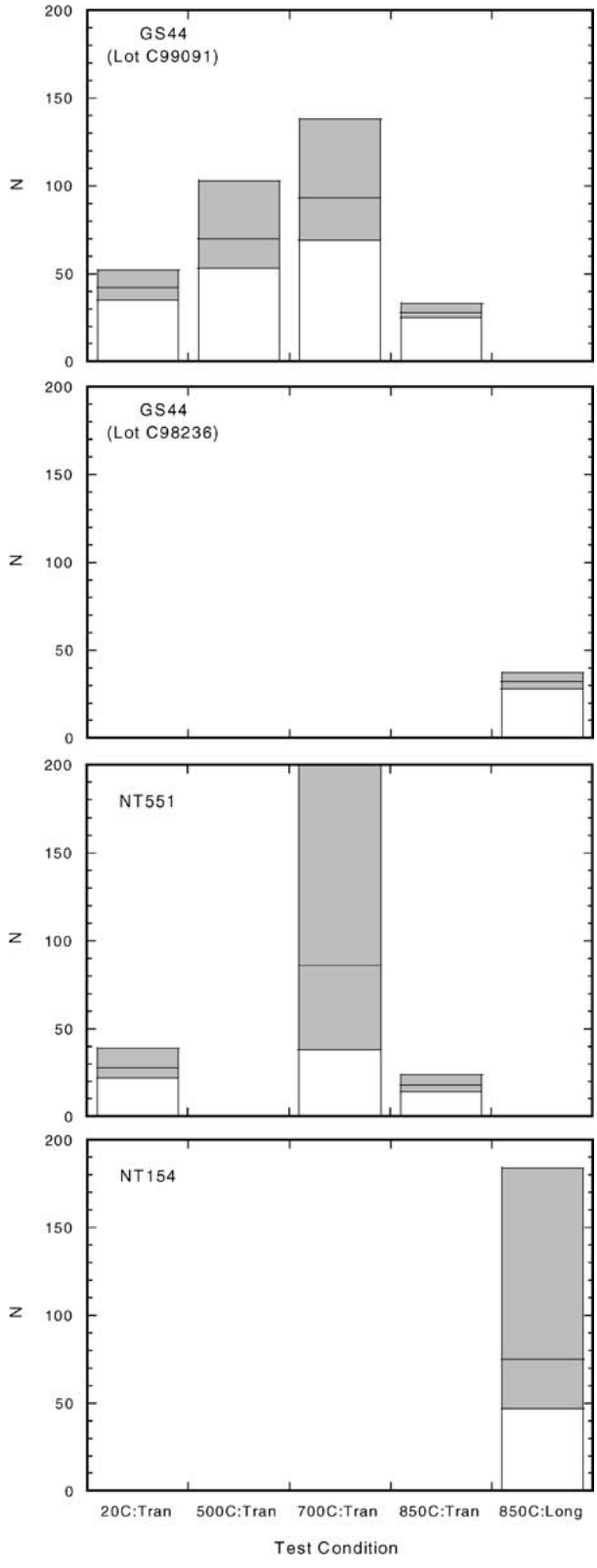

Figure 5 Slow crack growth exponent, N, as a function of test condition.

a change in material state and a change in the dominant failure mechanism in both ceramics. The fatigue exponent for NT154 was relatively large-valued compared to GS44 and NT551 indicating that such a change in material state was not a prevalent in it as for the two GPS silicon nitrides.

The authors exercise caution here in the interpretation of the quantified fatigue exponent values at 850°C. Because the dominant strength-limiting flaw apparently changed (was a function of stressing rate) at 850°C, the fatigue exponent using ASTM C1368 [19] is somewhat meaningless because its determination is predicated on the assumption that the fatigue mechanism is not dependent on the stressing rate. However, its value provides qualitative insight nonetheless, and its change between 700 and 850°C in of itself is illustrative of the change in fatigue mechanism.

Possible causes of these changes in dynamic fatigue susceptibility as a function of temperature were explored (to be described in Section 2.3.) with studies involving the use of RLOM and SEM, and XRD and DTA.

3.2. Change in material state or dominant failure mechanism

Fractography results generated with RLOM and SEM showed that a change in fracture behavior and microstructure occurred between 700 and 850°C for the GS44 and NT551: this coincided with the dramatic decrease in dynamic fatigue exponent for these two materials between the same temperature range. NT154 did not undergo an obvious change in fracture behavior between 20 and 850°C, and the authors believe that this is not a coincidence due to the fact that its fatigue exponent did not appreciably change in this temperature range either. These observations were the first evidence the authors observed that suggested that changes in material state (or change in dominant failure mechanism) were occurring in the GS44 and NT551 between 700 and 850°C, and that no change was occurring in the NT154 below 850°C.

These changes in fracture behaviors and microstructures for the GS44, NT551, and NT154 are shown in Fig. 6a–c, respectively. The upper four RLOM images in Fig. 6a and b and upper two in Fig. 6c show a comparison of the original fracture surfaces of the bend bar specimens which had strengths approximately equal to the characteristic strength for their respective test sets. For example, the GS44 had a characteristic strength of 694 MPa when it was tested at 700°C and 30 MPa/s; the shown GS44 specimen in Fig. 6a had a strength of 696.6 MPa. This approach to facilitate comparisons was deemed logical and was chosen to qualitatively compare fracture surfaces because their generated surfaces could then be referenced against a comparable strength (i.e., characteristic strength) among each set. Changes in fatigue exponent were a consequence of strength reduction occurring when specimens were tested at the slowest stressing rate (0.003 MPa/s), so microstructures on the surfaces of fractured bend bars were explored by the authors at this slow stress rate; their inspections were believed to offer the best opportunity to view any evidence of microstructural changes that were a consequence of a change in material state. In-depth comparisons of specimens tested at 20°C were deemed unnecessary as their fracture surfaces and microstructures from bars tested at 30 and 0.003 MPa/s were indistinguishable. The lower two images in Fig. 6a and b and bottom image in Fig. 6c show high magnification SEM images of the grain and grain boundary structures that resulted from testing at 0.003 MPa/s at 700°C or 850°C or both.

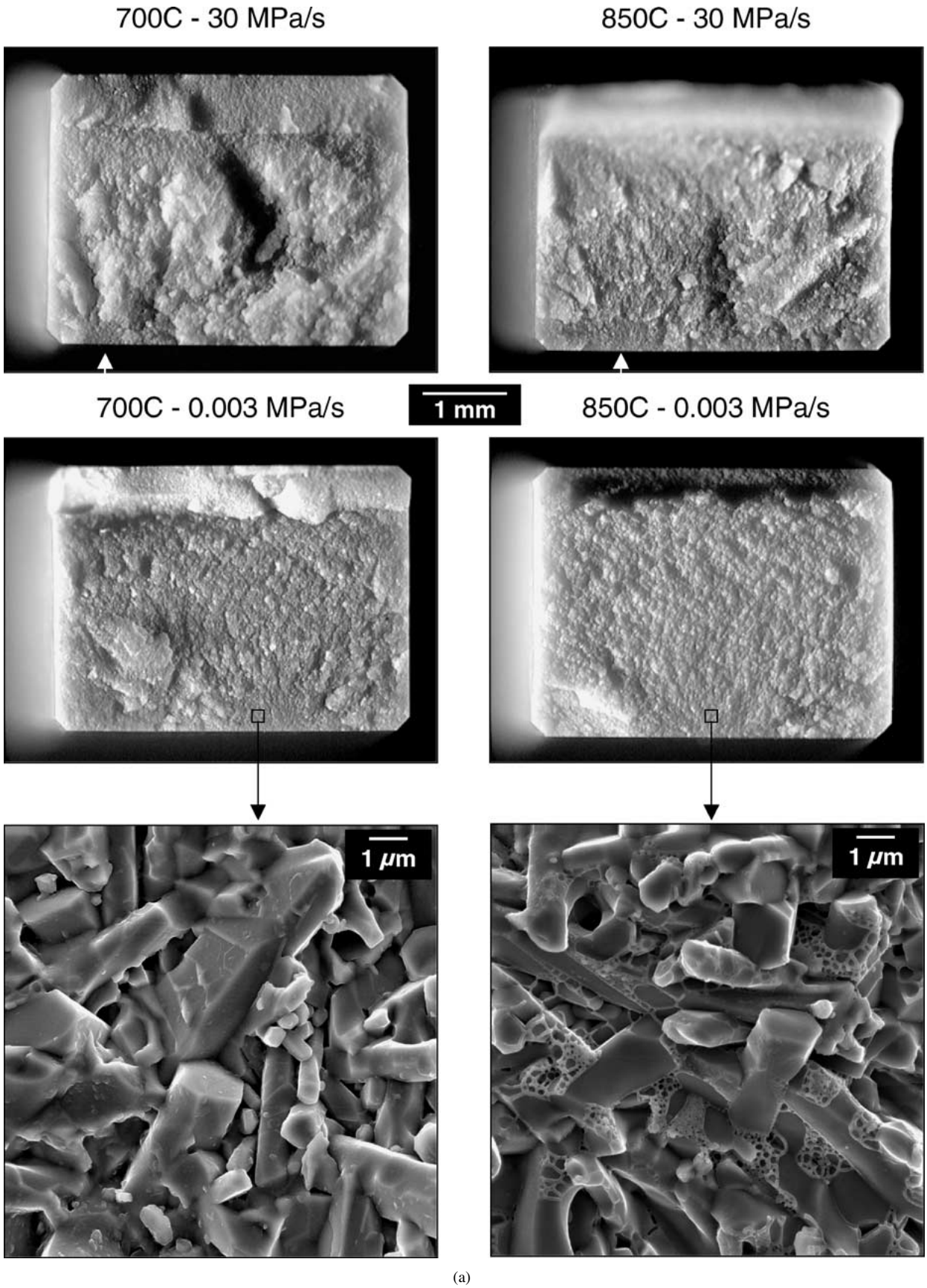

(a)

Figure 6 Bend bar fracture surfaces of (a) GS44, (b) NT551, and (c) NT154 as a function of test condition, and their microstructures at failure when tested at 0.003 MPa/s. The tensile surfaces of all the bend bars are oriented at the bottom as shown. Arrows in the top pictures of (a–c) indicate location of failure initiation. (*Continued.*)

The primary fracture surfaces of GS44 and NT551 bend bars tested at 700°C show a subtle increase in the mirror size upon comparison of bars tested at 30 MPa/s versus 0.003 MPa/s, while the mirror size on fracture surfaces of bars tested at 850°C were dramatically larger (and the qualitative fracture patterns in general were different too) for those tested at 0.003 MPa/s than at 30 MPa/s (see Fig. 6a and b). These trends in changing mirror sizes are representative of the strength decreases and are further reflective of the change in

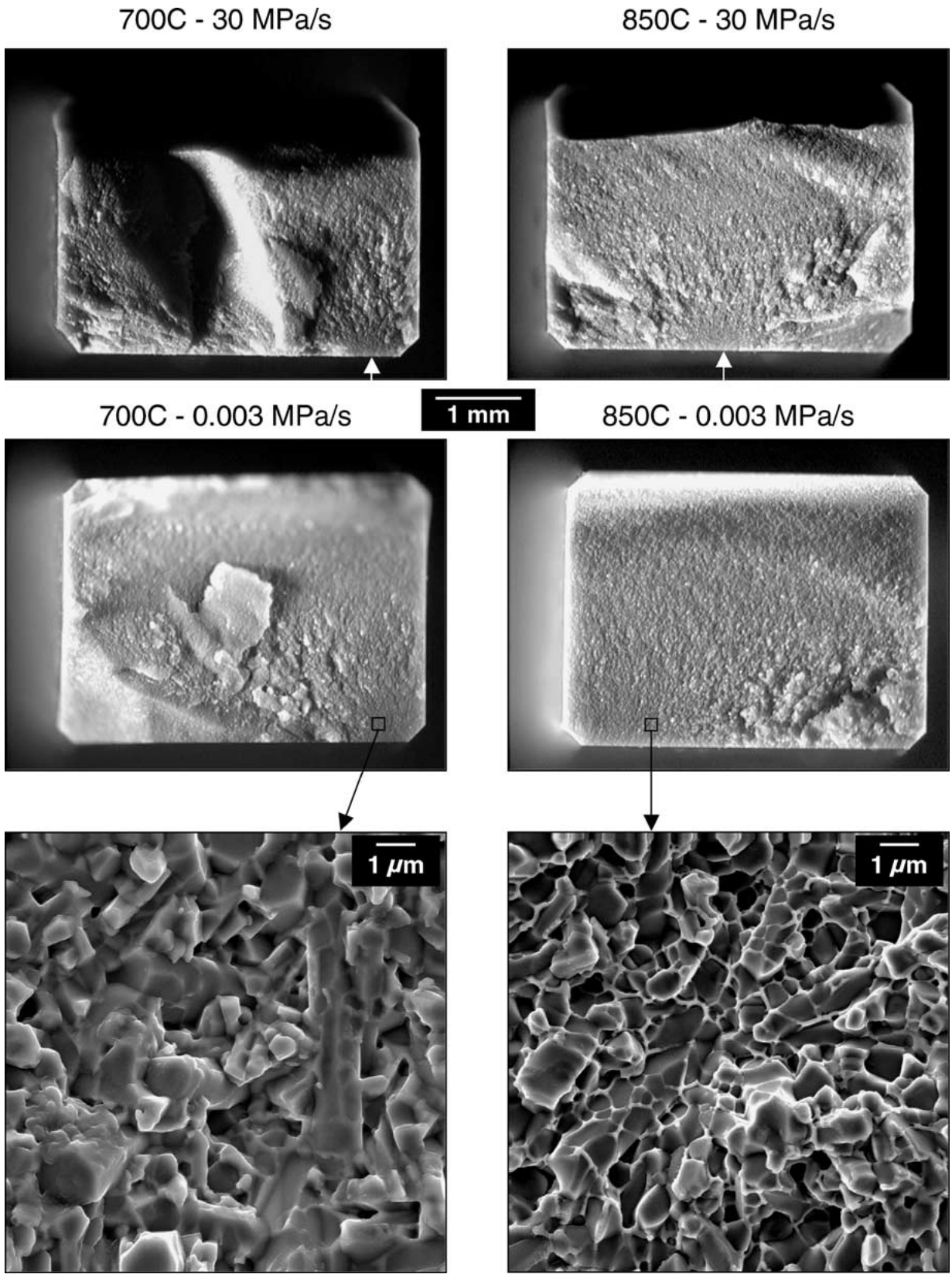

(b)

Figure 6 (*Continued.*)

material state in GS44 and NT551 that occurred between 700 and 850°C.

When those trends in mirror sizes on original fractures of GS44 and NT551 bend bars are compared to mirrors on NT154 fractured surfaces (see Fig. 6c), it is observed that the mirrors on fracture surfaces generated at 850°C are not dissimilar at 30 and 0.003 MPa/s for the NT154. This independence of fracture processes on the stressing rate at 850°C is illustrative of NT154 not undergoing a similar degree of change-in-material state that the GS44 and NT551 silicon nitrides exhibited below 850°C.

Microstructural investigations of the specimens shown in Fig. 6a–c revealed that the physical appearance of the secondary phase in GS44 and NT551 had changed as a consequence of increased test temperature

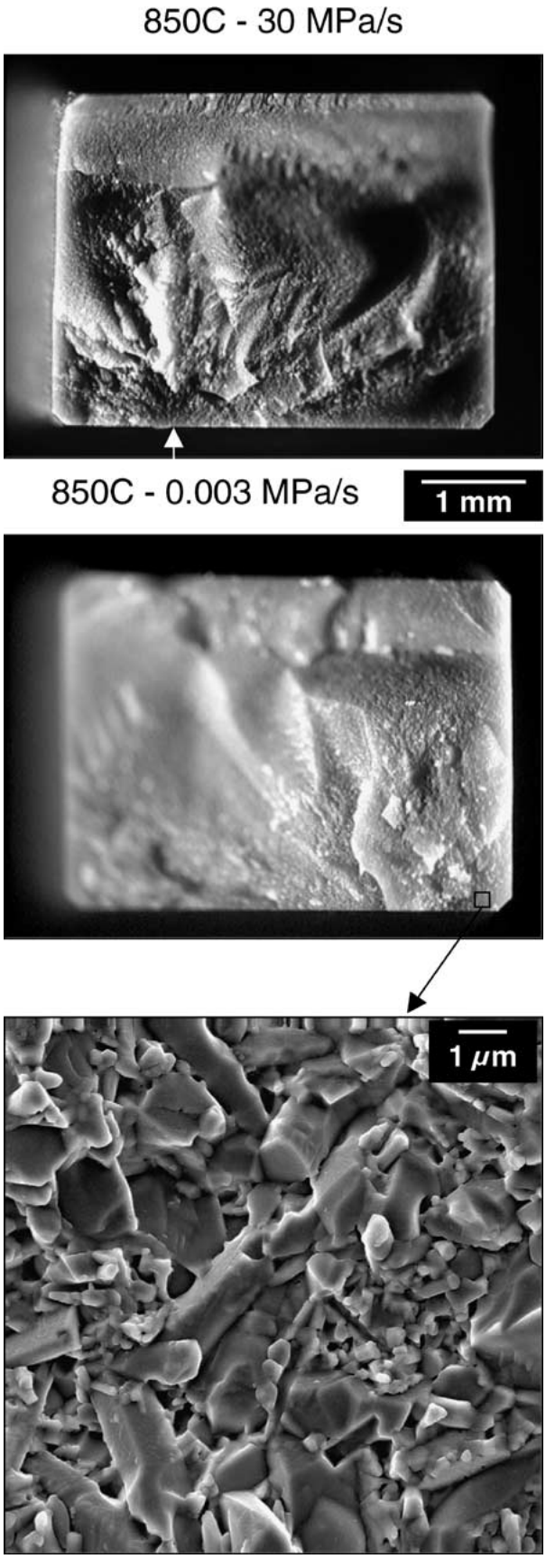

(c)

Figure 6 (*Continued.*)

to 850°C from 700°C when tested at 0.003 MPa/s, and that that for NT154 had not. The grain boundary phase in GS44 typically had imprinted or skeleton markings like that shown in Fig. 6a in bend bars tested at 850°C and 0.003 MPa/s, but did not when tested at 700°C. Though not as dramatic, the secondary phase in NT551 showed similar markings in bend bars tested at 850°C but too not at 700°C. The NT154 was not tested at 700°C; however, the physical appearance of its secondary phase was essentially unchanged from that generated during 20°C fractures. The changes in the appearance of the secondary phases in GS44 and NT551 between 700 and 850°C indicate that the material state of these two silicon nitrides had changed between those temperatures, and that that for the NT154 had not. The nature of the changes in 850°C testing at 0.003 MPa/s suggest softening of the secondary phase had occurred; however, if it indeed had occurred, then it did not have a structural effect on the GS44 and NT551 at 850°C because its effect did not manifest itself in non-linearity of the load-displacement curves for their tests (all such curves were linear to fracture).

The changes-in-material-state was not a consequence of any observable phase changes. X-ray diffraction spectra are shown in Fig. 7 for the GS44, NT551, and

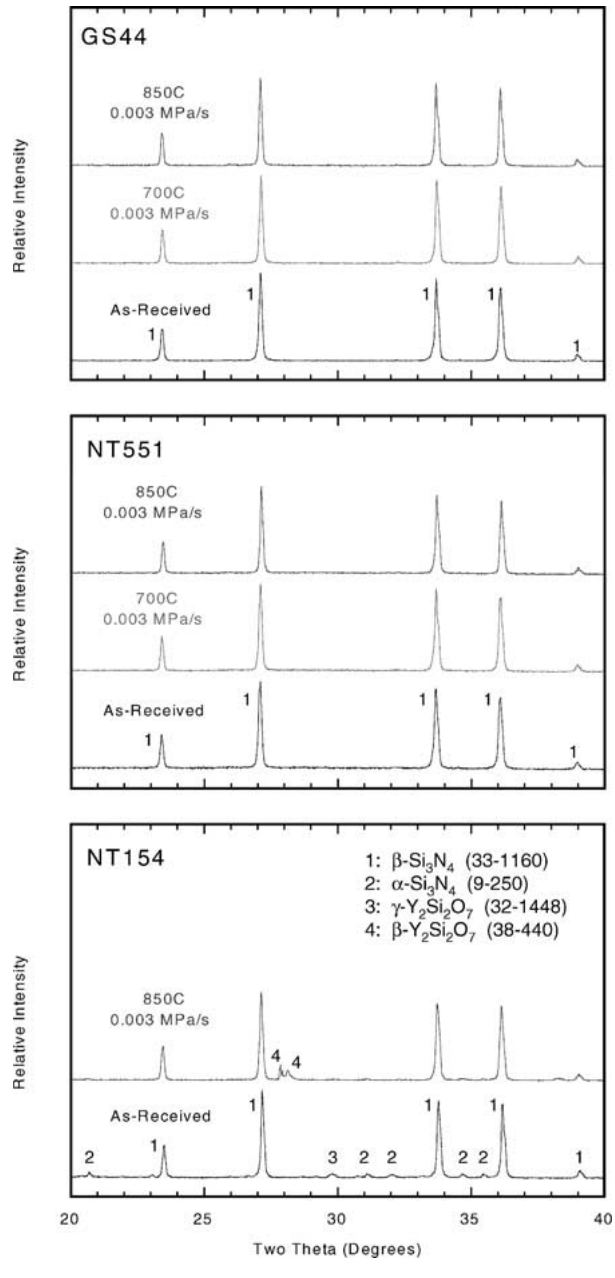

Figure 7 Phase content as a function of temperature.

NT154 tested at 20 and 850°C, and for the former two materials tested at 700°C. The spectra for the GS44 at 20, 700, and 850°C are the same as are those for the NT551. This shows that the changes in material state for the GS44 and NT551 to 850°C are not indicated by XRD. There was no longer α-Si_3N_4 in the NT154 as a consequence of testing at 850°C; however, its change did not appear to have any correlation or effect on dynamic fatigue susceptibility in NT154 (as it did not appreciably change).

A probable contributor to the change in material state (or change in failure mechanism) is oxygen diffusion into the silicon nitride via the grain boundaries and its effect on viscosity. Oxygen diffusion into the amorphous oxynitride grain boundaries increases the oxygen-to-nitrogen ratio and that acts to decrease its viscosity [22–24] at a given temperature. Because the diffusion process is active through the surface, the level of oxygen concentration is greatest at the surface and decreases toward a steady-state amount in the bulk. Flexure testing applies the greatest amount of tensile stress at the surface; consequently; changes in secondary phase viscosity and its effects are well exploited, even exaggerated, via this mechanical test. Effects of such oxidation, at least at high temperatures, have been deterministically studied in uniaxial tension and conclusively can be a lifetime limiter in silicon nitride [25]. The GS44 and NT551 had amorphous secondary phases in their grain boundaries, while the NT154's secondary phase was crystalline; therefore, if oxygen diffusion was a contributor to near-surface-viscosity-decreases in the grain boundaries, then that effect would be more marked in the GS44 and NT551 than in the NT154. A less viscous secondary phase will locally increase the material compliance and affect how crack propagation occurs, and conceivably can activate a different, locally non-elastic, failure process. Such a process would probably not be detectable in a load-displacement curve (especially in load control), nor would it manifest itself in macroscopic specimen curvature unless the viscosity was extremely low.

Although the effect of oxygen diffusion on material state (and subsequent time-dependent strength reduction) in silicon nitride at the temperatures explored in this study is speculative, it is not without ground. Oxidation processes at higher temperatures of several hundred degrees in silicon nitrides have been shown to lessen fatigue resistance [26, 27]. When those silicon nitrides were tested in non-oxidizing environments at equivalent temperatures, the detrimental effects associated with oxidation were non-existent [27]. Clearly the kinetics of oxidation (and the deleterious effects associated with it) are much more rapid as temperature is increased; however, the authors believe those kinetics are active at 850°C albeit much more sluggish.

The interpretation or validity of "inert strength" was perhaps compromised by the observed change in material state. Although 100% fractography was not performed, machining damage tended to be the dominant strength-limiting flaw for all specimens tested at 20, 700, and 850°C at 30 MPa/s (inert test condition). However, the authors speculate that a mechanism associated with oxidation and viscous deformation of the secondary phase at 850°C and 0.003 MPa/s was the dominant strength-limiting flaw in the GS44 and NT551. This change in mechanism did not alter the Weibull modulus in GS44; however, such a change in mechanism often does indeed cause the Weibull modulus to change with other silicon nitrides [28, 29]. The fact that a change in mechanism occurred also suggests that 30 MPa/s testing at 850°C perhaps did not yield an "inert" strength; however, a faster test rate was not examined so this cannot be concluded.

Perhaps the most striking observation of the supplemental characterizations was an ability of dilatometry to identify a transition that correlated to a change in material state and the observed changes in strength distribution. Specimen elongation and continuous CTE are shown as functions of temperature in Fig. 8 for GS44, NT551, and NT154. The transient change in the CTE of the GS44 and NT551 below approximately 400°C may be illustrative of that residual stress relief that was described in Section 3.1.2. A strong inflection in the CTE curve exists for the GS44 and NT551 at temperatures between 700 and 850°C, yet, such an inflection is absent from the CTE curve for NT154. Based on the

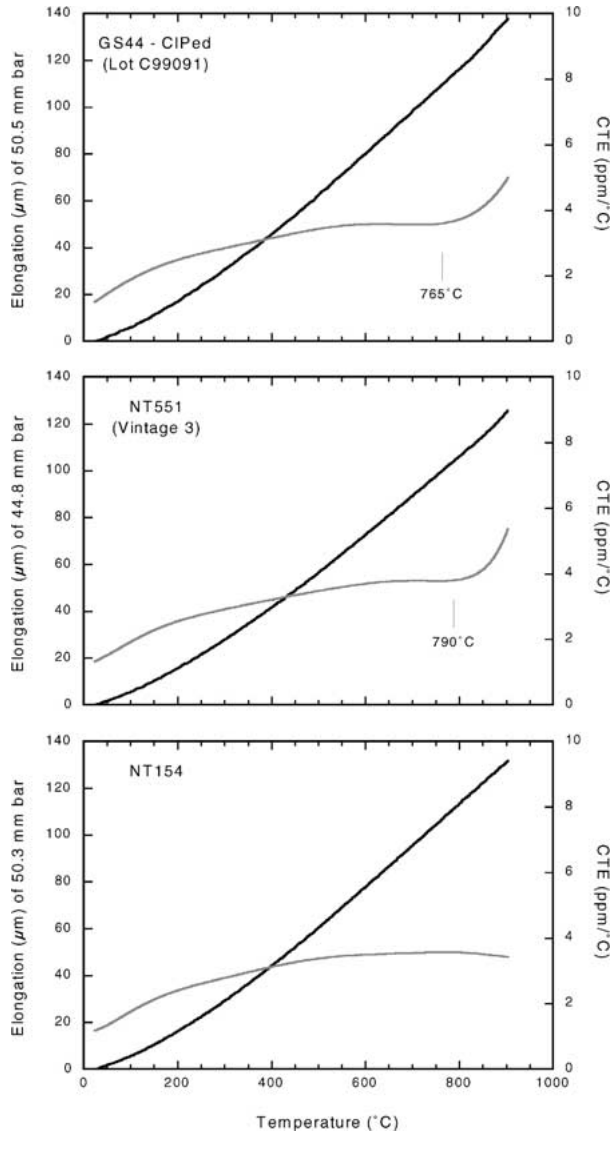

Figure 8 Coefficient of thermal expansion as a function of temperature.

strength distribution and microstructural changes that occurred in GS44 and NT551 between 700 and 850°C, the authors believe that the measurement of this CTE inflection is an indicator of those changes in material state that occurred in GS44 and NT551 which consequently affected their strength and fatigue susceptibility. The absence of such a CTE inflection below 850°C for NT154 and the fact that it was largely insusceptible to dynamic fatigue at 850°C is consistent with that observation.

Other commercial silicon nitrides having secondary phases and processed similar to GS44 and NT551 (both in silicate chemistries and volume fraction, and being gas pressure or pressureless sintered) examined by the authors show a decrease in uncensored inert characteristic strength with increasing temperature between 20 and 850°C too [30, 31]. Additionally, those same silicon nitrides exhibited a CTE inflection below 850°C like that shown in Fig. 8 for GS44 and NT551. Conversely, the silicate secondary phase in NT154 silicon nitride: was fully crystalline and stable in an ambient environment; was non-continuous and fully segregated at multigrain junctions, and; comprised a relatively low volume fraction of the whole material (compare its microstructure to that of GS44 and NT551 shown in Fig. 1). NT154 was hot isostatically pressed, and many of these secondary phase characteristics can only be achieved when silicon nitride is processed via this route. In further support of the existence of a correlation between the presence of a significant CTE inflection and a decrease in fatigue resistance, there was not a significant change in CTE in HIPed SN235 silicon nitride below 850°C and it exhibited high slow crack growth resistance to that temperature [31].

Govila [32] observed a similar strength decrease in an yttria-doped silicon nitride at these intermediate temperatures and attributed it to oxidation-induced microcracking; however, that silicon nitride's grain boundaries contained crystalline yttrium silicates that have been shown to undergo relatively large volumetric changes when oxidized [33, 34]. None of the examined silicon nitrides in this study contained these same grain boundary phases.

We therefore conclude that such CTE analysis is an effective, quick, and inexpensive screening test to predict whether or not a prospective candidate silicon nitride will be susceptible to dynamic fatigue or changes in material state up to a prospective use temperature. Based on the results in the present study, we assert that the vintage of GS44 tested in the present study could be confidently used to approximately 750°C, that the vintage of NT551 examined could be confidently used to approximately to 780°C, and that the NT154 tested could be confidently used to at least 900°C without a dramatic increase in fatigue susceptibility.

4. Conclusions

The flexure strength distributions and dynamic fatigue of GS44, NT551, and NT154 silicon nitrides were determined at intermediate temperatures (≤850°C) in ambient air. The inert characteristic strength for the GS44 and NT551 decreased with temperature while that for the NT154 was statistically independent of temperature. The slow crack growth exponent, N, for the GS44 and NT551 exhibited a 70–80% decrease between 700 and 850°C while the strength of NT154 was comparatively independent of stressing rate at 850°C. Associated with that, the coefficient of thermal expansion (CTE) for the GS44 and NT551 sharply increased between 700 and 850°C while that for the NT154 did not.

Although the presence of a relatively large change in CTE (and the temperature range where it occurred) did not have any obvious correlation with a change in inert strength at these intermediate temperatures, it appears to occur at a temperature where there is an associated change in: dominant failure mechanism; the uncensored characteristic strength or uncensored Weibull modulus or both, and; the fatigue exponent. This inflection in the CTE dependence on temperature occurs at a temperature where there is a change in material state that is linked to the equilibrium state of the secondary phase in silicon nitride.

Acknowledgments

Research was sponsored by the U.S. Department of Energy, Assistant Secretary for Energy Efficiency and Renewable Energy, Office of Transportation Technologies, as part of the Heavy Vehicle Propulsion System Materials Program, under Contract DE-AC05-00OR22725, managed by UT-Battelle, LLC. The authors wish to thank G. Gilde and J. Swab for reviewing the manuscript and for their helpful comments, and C. J. Rawn for performing the XRD experiments.

References

1. D. W. RICHERSON, "Modern Ceramic Engineering" (Marcel Dekker, New York, NY, 1982).
2. R. KAMO and W. BRYZIK, *Society of Automotive Engineers (SAE)* **SP-571** (1984) 21.
3. M. SCHREINER, W. LIANG, R. KAMO and R. WALSON, SAE Paper No. 870418, 1987.
4. M. ASNANI and F. KUONEN, SAE Paper No. 850358, 1988.
5. D. H. UPDIKE and P. D. NAGLE, SAE Paper No. 880441, 1988.
6. D. M. KABAT, I. J. GARWIN and D. L. HARTSOCK, SAE Paper No. 880670, 1988.
7. R. R. WILLS, *Communications of the American Ceramic Society* **72** (1988) 1261.
8. Y. HORI, Y. MIYAKAWA, S. ASAMI and T. KAJIHARA, SAE Paper No. 890175, 1989.
9. G. RODGERS, R. SOUTHAM, J. REINICKE-MURMANN and P. KREUTER, SAE Paper No. 900452, 1990.
10. R. HAMMINGER and J. HEINRICH, J., in "Proceedings of the Materials Research Society Symposia" (1993) Vol. 287, p. 513.
11. H. IZUMIDA, T. NISHIOKA, A. YAMAKAWA and M. YAMAGIWA, SAE Paper No. 970003, 1997.
12. N. N. NEMETH, L. M. POWERS, L. A. JANOSIK and J. P. GYEKENYESI, 1993, Users and Programmers Manual, NASA TP-2916, National Aeronautics and Space Administration, Cleveland, OH, 1993.
13. AlliedSignal Engines (Phoenix, AZ), ORNL/Sub/89-SC674/1-2, DOE Office of Transportation Technologies, 1995.
14. A. A. WERESZCZAK, T. P. KIRKLAND, M. K. FERBER and M. J. ANDREWS, *Ceramic Engineering and Science Proceedings* **18** (1997) 475.
15. M. J. ANDREWS, A. A. WERESZCZAK and K. BREDER, *ibid.* **20** (1999) 555.
16. M. N. MENON, H. T. FANG, D. C. WU, M. G. JENKINS, M. K. FERBER, K. L. MORE, C. R. HUBBARD and T. A. NOLAN, *J. Amer. Ceram. Soc.* **77** (1994) 1217.

17. ASTM C1161, in "Annual Book of ASTM Standards," Vol. 15.01 (American Society for Testing and Materials, West Conshohocken, PA, 1999).
18. ASTM C1239, in "Annual Book of ASTM Standards," Vol. 15.01 (American Society for Testing and Materials, West Conshohocken, PA, 1999).
19. ASTM C1368, in "Annual Book of ASTM Standards," Vol. 15.01 (American Society for Testing and Materials, West Conshohocken, PA, 1999).
20. ASTM E228, in "Annual Book of ASTM Standards," Vol. 14.02 (American Society for Testing and Materials, West Conshohocken, PA, 1999).
21. G. W. HOLLENBERG, G. R. TERWILLIGER and R. S. GORDON, *J. Amer. Ceram. Soc.* **54** (1971) 196.
22. S. HAMPSHIRE, R. DREW and K. H. JACK, *ibid.* **67** (1984) C46.
23. S. SAKKA, *Annual Review of Materials Science* **16** (1986) 29.
24. E. Y. SUN, P. F. BECHER, S.-H. HWANG, S. B. WATERS, G. M. PHARR and T. Y. TSUI, *Journal of Non-Crystalline Solids* **208** (1996) 162.
25. A. A. WERESZCZAK, M. K. FERBER, T. P. KIRKLAND, K. L. MORE, M. R. FOLEY and R. L. YECKLEY, *J. Amer. Ceram. Soc.* **78** (1995) 2129.
26. A. A. WERESZCZAK, K. BREDER and M. K. FERBER, *ibid.* **76** (1993) 2919.
27. A. A. WERESZCZAK, T. P. KIRKLAND, K. BREDER, M. K. FERBER and P. KHANDELWAL, *Materials Science and Engineering* A **191** (1995) 257.
28. A. WERESZCZAK, K. BREDER, M. J. ANDREWS, T. P. KIRKLAND and M. K. FERBER, ASME Paper No. 98-GT-527, presented at International Gas Turbine and Aeroengine Congress and Exhibition, Stockholm, Sweden, June 2–5, 1998.
29. K. BREDER, A. A. WERESZCZAK and M. J. ANDREWS, *Ceramic Engineering and Science Proceedings* **19** (1998) 89.
30. A. A. WERESZCZAK, T. P. KIRKLAND, H.-T. LIN and S. K. LEE, *ibid.* **21** (2000) 497.
31. A. A. WERESZCZAK, T. P. KIRKLAND, H.-T. LIN, R. A. OTT, C. R. BRINKMAN, S. K. LEE, M. J. ANDREWS and J. THIELE, Heavy Vehicle Propulsion System Materials Program Semiannual Technical Progress Report, DOE Office of Transportation Technologies, Oct. 1999–Mar. 2000, pp. 82–90 in Oak Ridge National Laboratory Report No. ORNL/TM-2000/233, August 2000.
32. R. T. GOVILA, *American Ceramic Society Bulletin* **65** (1986) 1287.
33. F. F. LANGE, S. C. SINGHAL and R. C. KUZNICKI, *J. Amer. Ceram. Soc.* **60** (1977) 249.
34. K. E. AMIN, K. N. SIEBEIN and J. A. WADE, *J. Mater. Sci.* **24** (1989) 4253.

Received 14 August 2001
and accepted 25 February 2002